3D Radio Map Reconstruction based on Generative Adversarial Networks under Constrained Aircraft Trajectories

Tianyu Hu, Yang Huang, Junting Chen, Qihui Wu, Zhiren Gong

***Abstract*—Three-dimensional (3D) radio map, which characterizes the spatial distribution of the received signal strength (RSS) across a 3D space, can be a significant tool for wireless resource management and spectrum surveillance. However, incomplete 3D radio map is usually obtained in practice due to the infinite number of positions where aircraft perform RSS measurement suffering from constrained trajectories. In order to tackle this problem, we propose a 3D radio map reconstruction scheme based on generative adversarial networks (GANs), where a novel GAN variant with unsupervised learning is proposed. Specifically, the cost function of the variant integrates a reconstruction loss and an adversarial loss, while the network structure exploits ResNet and dilated convolution under the idea of patchGAN. Numerical results reveal that the network structure and the cost function can benefit the reconstruction scheme, yielding low-volatility and lower average mean squared error (MSE). Moreover, it is shown that the proposed scheme can outperform various baselines in terms of the average MSE, even if the number of measured samples for inference significantly decreases.**

***Keywords*—3D radio map reconstruction, generative adversarial networks, constrained aircraft trajectories, deep learning.**

I. Introduction

RADIO map characterizes the spatial distribution of the received signal strength (RSS) across a geographic space of interest, and has already been leveraged to optimize the deployment of vehicular base stations, manage interference and guarantee spectrum security for terrestrial wireless networks [1]–[3]. Nevertheless, the application of aircraft (e.g. drones) in enhanced mobile broadband, massive machine-type communications and radio-based sensing [4], [5] makes radio maps, which are constructed with RSS measured on the ground, inapplicable to wireless resource management and spectrum surveillance in a air-ground three-dimensional (3D) space. Aircraft mounted with spectrum monitoring device (SMD) can be used to measure the RSS in the 3D space. In practice, it is not possible to collect RSS measurements for all possible positions in the 3D space. As a result, it is vital but challenging to reconstruct 3D radio maps from a sparse subset of measurements over the 3D space.

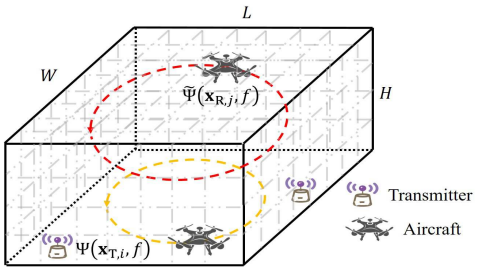

Fig. 1. The flying scenario of the aircraft.

Indeed, classic spatial interpolation algorithms such as inverse distance weighted (IDW) [6] and kriging [7] algorithms might be extended for 3D radio map reconstruction. However, the kriging algorithm is difficult to implement in the multiple transmitter scenario where the spatial statistics of the RSS is non-stationary, in which case, the computational complexity and the required measurement data are overwhelming [7]. Furthermore, the IDW algorithm takes the distance between transceivers as the only factor that affects the RSS, while neglects the effects of key wireless channel characteristics such as shadow fading on the RSS. Therefore, in order to tackle the aforementioned issues for 3D radio map reconstruction, novel signal processing skills are in demand.

Prior work in [8] reconstructed a 3D radio map by averaging the measured RSS samples in a straight-forward manner, while the authors in [9] proposed a total variance based 3D radio map reconstruction (3DTV-SMR) algorithm to improve the reconstruction accuracy. However, the trajectory planned for sampling the RSS in [8] is evenly distributed in the entire space, such that the SMD measures at almost all positions. In [9], an ideal trajectory is optimized without any constraint on the flight path, such that the achieved trajectory is densely distributed in the 3D space. It can be drawn from the aforementioned works that the methods therein require spatially dense measurement samples which incur a huge cost for aircraft to follow the designed trajectory. In contrast to the above studies, in practice, the trajectories of aircraft can be subject to flight plan, flight restricted zones, turning radius, etc. Therefore, this paper investigates 3D radio map reconstruction considering constrained trajectories, which are preset but not optimized for improving the reconstruction accuracy. specifically, we consider that the aircraft fly along several circle flight circuits with different radii and altitudes to perform measurement, as depicted in Fig. 1.

This work was partially supported by the National Natural Science Foundation of China under Grant 61901216, U2001210 and 61827801, the Natural Science Foundation of Jiangsu Province under Grant BK20190400. (Corresponding author: Yang Huang)

T. Hu, Y. Huang, Q. Wu and Z. Gong are with the Key Laboratory of Dynamic Cognitive System of Electromagnetic Spectrum Space, Ministry of Industry and Information Technology, Nanjing University of Aeronautics and Astronautics, Nanjing, 210016, China (e-mail: {huty, yang.huang.ceie, ZhirenGongi}@nuaa.edu.cn; wuqihui2014@sina.com). J. Chen is with the Chinese University of Hong Kong, Shenzhen (email: juntingc@cuhk.edu.cn).

As a generative framework of deep learning (DL), Generative adversarial networks (GANs) [10] has attracted intensive research interests in wireless communication [11], [12]. GANs feature the ability of capturing the distribution of actual dada and generating mimic samples conforming to the captured distribution. This is reminiscent of exploiting GANs to capture the distribution of the RSS, such that the entire 3D radio map, which is generated by the GAN and almost identical to the actual complete 3D radio map, can be reconstructed. Motivated by this, we propose a 3D radio map reconstruction scheme based on GANs.

Furthermore, for the sake of a more practical design, we assume that GANs can only be trained with the incomplete 3D radio maps (which can be obtained through local historical data or online monitoring), while the corresponding actual complete maps cannot be utilized during training. In other words, there is no access to the complete 3D radio map. Due to this, during the training process of a conventional GAN [10], the GAN cannot evaluate the quality of the reconstructed 3D radio map generated by itself. In order to address this problem, unsupervised learning [13] is exploited in our proposed scheme. Besides, we also propose a novel GAN variant, by integrating GAN with the 3D-dilated convolution and ResNet, so as to improve the learning ability and the training stability of GANs. The proposed GAN variant is then referred to as 3D-DCRGAN. Simulation results reveal that the training of the 3D-DCRGAN can benefit from a carefully designed cost function consisting of a reconstruction loss and an adversarial loss, yielding lower average mean squared error (MSE) for radio map reconstruction. Additionally, the proposed scheme can outperform conventional methods such as IDW and 3DTV-SMR, in terms of the average MSE, even if the amount of measured data for inference significantly decreases.

II. Preliminaries

1) System Model: We consider that there are N_{T} transmitters in the 3D target space $\mathbf{A}$ with dimensions $L \times W \times H$. We divide the space $\mathbf{A}$ into $N_{\mathrm{G}} = N_{\mathrm{L}} \times N_{\mathrm{W}} \times N_{\mathrm{H}}$ grids and assume that there is at most one transmitter within an arbitrary grid. Specifically, the grid position (which means the location of an item on the grid) and the transmit power of the i th transmitter are denoted as $\mathbf{x}_{\mathrm{T},i} \in \mathbb{R}^3$ and $\Psi\left(\mathbf{x}_{\mathrm{T},i}, f\right)$ respectively, where f is the frequency point of interest.

Moreover, we assume that signal propagation function $\Gamma_{\mathbf{x}_{\mathrm{T},i} \to \mathbf{x}}(f)$ follows the log-distance path loss model, where $\mathbf{x} \in \mathbb{R}^3$ is the grid position of interest. That is, the path loss $PL(d, f)$ (dB) from the i th transmitter to position $\mathbf{x}$ can be expressed as $PL(d, f) = P_{\mathrm{FREE}}\left(d_0, f\right) + 10n \log\left(\frac{d}{d_0}\right) + X_\eta$, where d, d_0 and n are the distance between $\mathbf{x}_{\mathrm{T},i}$ and $\mathbf{x}$, reference distance and path loss exponent, respectively. Note that the term $P_{\mathrm{FREE}}(d_0, f)$ is the free space path loss at d_0, and the term $X_\eta \sim \mathcal{N}(0, \eta^2)$ characterizes the shadow fading with unit of dB. Therefore, the RSS $\Psi(\mathbf{x}, f)$ at position $\mathbf{x}$ can be obtained by $10 \log \Psi(\mathbf{x}, f) = 10 \log \Psi\left(\mathbf{x}_{\mathrm{T},i}, f\right) - PL(d, f)$.

2) Problem Formulation: A 3D radio map of space $\mathbf{A}$ can be characterized by a function mapping from a 2-tuple variable $(\mathbf{x}, f)$ to the RSS $\Psi(\mathbf{x}, f)$ [1]. We consider that the RSS at N_{R} grids (among the N_{G} grids) can be measured by aircraft under constrained trajectories. The measured RSS at the j th grid, denoted as $\widetilde{\Psi}\left(\mathbf{x}_{\mathrm{R},j}, f\right)$, is collected at the position $\mathbf{x}_{\mathrm{R},j}$ of gird j. Therefore, $\widetilde{\Psi}\left(\mathbf{x}_{\mathrm{R},j}, f\right) = \sum_{i=1}^{N_{\mathrm{T}}} \Gamma_{\mathbf{x}_{\mathrm{T},i} \to \mathbf{x}_{\mathrm{R},j}}(f) \Psi\left(\mathbf{x}_{\mathrm{T},i}, f\right) + \sigma^2$, where σ^2 represents the variance of the additive white Gaussian noise.

In practice, the RSS at each unmeasured grid $\mathbf{x}_{\mathrm{U}}$ is unknown, and based on this, we define an incomplete 3D radio map $\widetilde{\mathbf{\Psi}}(f) = \{\widetilde{\Psi}(\mathbf{x}, f) | \forall \mathbf{x} \in \mathbf{A}\}$, where the RSS value of each unmeasured grid is set to 0, e.g. $\widetilde{\Psi}\left(\mathbf{x}_{\mathrm{U}}, f\right) = 0$; and that of an arbitrary j th measured grid is $\widetilde{\Psi}\left(\mathbf{x}_{\mathrm{R},j}, f\right)$. Moreover, we define a reconstructed 3D radio map $\widehat{\mathbf{\Psi}}(f) = \{\widehat{\Psi}(\mathbf{x}, f) | \forall \mathbf{x} \in \mathbf{A}\}$, where each value $\widehat{\Psi}(\mathbf{x}, f)$ is equal to either an estimated RSS $\widehat{\Psi}(\mathbf{x}_{\mathrm{U}}, f)$ (for an unmeasured grid) or $\widetilde{\Psi}\left(\mathbf{x}_{\mathrm{R},j}, f\right)$ (for a measured grid). Furthermore, we define a complete 3D radio map $\mathbf{\Psi}(f) = \{\Psi(\mathbf{x}, f) | \forall \mathbf{x} \in \mathbf{A}\}$, which is a true map from a god's-eye view but unavailable in practice, i.e. each grid is measured by the aircraft.

A distortion function is defined to evaluate the reconstruction accuracy. Given the complete map $\mathbf{\Psi}(f)$ and the reconstructed map $\widehat{\mathbf{\Psi}}(f)$, the distortion function can be defined as an MSE given by $\frac{1}{N_{\mathrm{G}}} \sum_{\mathbf{x} \in \mathrm{A}} (\Psi(\mathbf{x}, f) - \widehat{\Psi}(\mathbf{x}, f))^2$. Hence, the 3D radio map reconstruction problem is formulated as

$$\min_{\widehat{\mathbf{\Psi}}} \ \frac{1}{N_{\mathrm{G}}} \sum_{\mathbf{x} \in \mathrm{A}} (\Psi(\mathbf{x}, f) - \widehat{\Psi}(\mathbf{x}, f))^2 \tag{1}$$

$$\text{s.t. } \widehat{\Psi}(\mathbf{x}_{\mathrm{R},j}, f) = \widetilde{\Psi}\left(\mathbf{x}_{\mathrm{R},j}, f\right), \ j = 1, 2, \cdots, N_{\mathrm{R}}. \tag{1a}$$

Note that in the above equation, the values of N_{R}, $\mathbf{x}_{\mathrm{R},j}$ and $\widetilde{\Psi}(\mathbf{x}_{\mathrm{R},j}, f)$ are known, while those of N_{T}, $\mathbf{x}_{\mathrm{T},i}$ and $\Psi(\mathbf{x}_{\mathrm{T},i}, f)$ are unknown. Intuitively, solving the above reconstruction problem with such a formulation is reminiscent of GAN [14], while the unavailable complete radio map makes training a GAN intractable. In the subsequent discussions, we assume that the frequency point f is a given value unless otherwise stated. For notational simplicity, the complete map $\mathbf{\Psi}(f)$, the incomplete map $\widetilde{\mathbf{\Psi}}(f)$ and the reconstructed map $\widehat{\mathbf{\Psi}}(f)$ are designated as $\mathbf{\Psi}$, $\widetilde{\mathbf{\Psi}}$ and $\widehat{\mathbf{\Psi}}$, respectively.

III. Network Structure of 3D-DCRGAN

In order to perform 3D radio map reconstruction where complete 3D radio maps are unavailable during training, we integrate unsupervised learning with the proposed 3D-DCRGAN, which is composed of a generator network G with parameters θ_g (i.e., weights and biases of neurons) and a discriminator network D with parameters θ_d. In the following, we elaborate the reason of applying unsupervised learning. Due to the unavailability of a complete radio map, the input of the generator G has to be an incomplete map $\widetilde{\mathbf{\Psi}}$ and a latent variable $\mathbf{z} \sim \mathcal{N}(0, 1)$, such that the generator can output a reconstructed map $\widehat{\mathbf{\Psi}} = G(\mathbf{z} | \widetilde{\mathbf{\Psi}}; \theta_g)$. However, applying supervised or unsupervised learning can result in different input of the discriminator D. In order to perform supervised learning, a reconstructed map $\widehat{\mathbf{\Psi}}$, i.e. a mimic sample output by the generator G, and a complete map $\mathbf{\Psi}$, i.e. an actual sample known as the ground truth corresponding to the mimic sample $\widehat{\mathbf{\Psi}}$, have to be alternately used as the input of the discriminator D. Since it is hard to obtain the complete

map $\boldsymbol{\Psi}$ in practice, we have to utilize the incomplete map by performing unsupervised learning. Thus, the input of the discriminator D is designed to be an incomplete map $\widetilde{\boldsymbol{\Psi}}$ or a mimic incomplete map $\widetilde{\boldsymbol{\Psi}}_{\mathrm{m}} = \mathbf{M}_{\mathrm{b}} \odot \widehat{\boldsymbol{\Psi}}$, where $\odot$ represents the element-wise product operation and $\mathbf{M}_{\mathrm{b}}$ is a binary matrix with the element $m_{\mathrm{b}}(\mathbf{x}_{\mathrm{R},j}) = 1$ or $m_{\mathrm{b}}(\mathbf{x}_{\mathrm{U}}) = 0$. Note that the input of 3D-DCRGAN and the matrix $\mathbf{M}_{\mathrm{b}}$ need to be preprocessed by the proposed scheme, which will be elaborated in Section IV.

Moreover, there are two major challenges of designing an effective GAN variant for the 3D radio map reconstruction under constrained trajectories. Firstly, the complete 3D radio map cannot be used as a priori information for the designed GAN variant, while the variant needs to be able to capture the complete distribution of the RSS. Secondly, due to constrained aircraft trajectories, the number of measured grids might be very limited. Therefore, the proposed 3D-DCRGAN needs to be sophisticatedly designed, so as to improve GAN's ability of capturing the distribution of the RSS given the incomplete 3D radio map with very little useful information.

Therefore, in terms of the network structure of GANs, we first employ ResNet [15] to increase the number of convolutional layers, since ResNet is able to avoid training accuracy degradation due to an increase in network depth through residual connection. Moreover, we exploit dilated convolution [16] to increase the receptive field size, so as to compensate for the loss of contextual information affected by the downsampling process of convolutional layer. Note that a layer with dilated convolution is a convolutional layer with dilation factor $d_{\mathrm{c}} > 1$. In order to enhance the training stability, dilated convolution is integrated with ResNet to obtain residual blocks used in the discriminator D and the generator G of 3D-DCRGAN. In addition, when designing the discriminator D, we utilize the idea of PatchGAN [14] to comprehensively extract the information of the incomplete 3D radio map, such that the output of the discriminator D turns out to be a matrix where each element represents the discrimination result of each patch (i.e. a small cube containing $N_1 \times N_2 \times N_3$ grids) in the input. The network structure of the proposed 3D-DCRGAN is summarized in Fig. 2, where $h = (k, s_{\mathrm{c}}, p_{\mathrm{c}}, d_{\mathrm{c}})$ is a set of hyperparameters of the 3D convolutional layer or the 3D transposed convolutional layer, and b is the index of the residual block. Note that k, s_{c} and p_{c} are the kernel size, stride and padding of the layers, respectively.

IV. GAN-Based Reconstruction Scheme

This section proposes a 3D radio map reconstruction scheme based on 3D-DCRGAN. The proposed scheme consists of a preprocessing stage, an off-line unsupervised learning-based training stage and an online inference stage, where a novel cost function of the 3D-DCRGAN is proposed for training. Remarkably, the preprocessing should be performed prior to not only the off-line training but also the online inference.

A. Preprocessing Stage

At this stage, incomplete 3D radio maps are preprocessed to decrease the training complexity and improve the learning ability of 3D-DCRGAN. We first perform Max-Min normalization on each incomplete map, i.e. $\widetilde{\boldsymbol{\Psi}}_{\mathrm{n}} = \left\{\widetilde{\Psi}_{\mathrm{n}}(\mathbf{x}) = \frac{\widetilde{\Psi}(\mathbf{x}) - \widetilde{\Psi}_{\min}}{\widetilde{\Psi}_{\max} - \widetilde{\Psi}_{\min}} \middle| \forall \mathbf{x} \in \mathbf{A}, \widetilde{\Psi}(\mathbf{x}) \neq 0\right\}$, where $\widetilde{\Psi}_{\min}$ and $\widetilde{\Psi}_{\max}$ are the minimum and maximum values of RSS in historical data (or online monitoring data), respectively. Hence, a number of gray-scale incomplete maps, each with dimensions $1 \times N_{\mathrm{L}} \times N_{\mathrm{W}} \times N_{\mathrm{H}}$, can be obtained. However, it is easy to confuse a measured grid where $\widetilde{\Psi}_{\mathrm{n}}(\mathbf{x})|_{\widetilde{\Psi}(\mathbf{x})=\widetilde{\Psi}_{\min}} = 0$ with an unmeasured grid where $\widetilde{\Psi}(\mathbf{x}_{\mathrm{U}}) = 0$ in the gray-scale map. In order to handle this problem, overwriting is performed. That is, we first copy each gray-scale map and each corresponding binary matrix $\mathbf{M}_{\mathrm{b}}$ twice and obtain a three-channel map $\widetilde{\boldsymbol{\Psi}}_{\mathrm{t}} = [\widetilde{\boldsymbol{\Psi}}_{\mathrm{n}}, \widetilde{\boldsymbol{\Psi}}_{\mathrm{n}}, \widetilde{\boldsymbol{\Psi}}_{\mathrm{n}}]^T$ and the corresponding matrix $\mathbf{M}_{\mathrm{t}} = [\mathbf{M}_{\mathrm{b}}, \mathbf{M}_{\mathrm{b}}, \mathbf{M}_{\mathrm{b}}]^T$ with dimensions $3 \times N_{\mathrm{L}} \times N_{\mathrm{W}} \times N_{\mathrm{H}}$, respectively[1]. Then, each unmeasured grid in each map is colored in red (or other colors except black, white and gray). By this means, we can obtain a number of colored incomplete 3D radio maps, where each can be designated as $\widetilde{\boldsymbol{\Psi}}_{\mathrm{c}}$. The set that collects these maps is referred to as the training set for the off-line unsupervised learning-based training stage or the testing set for the online inference stage.

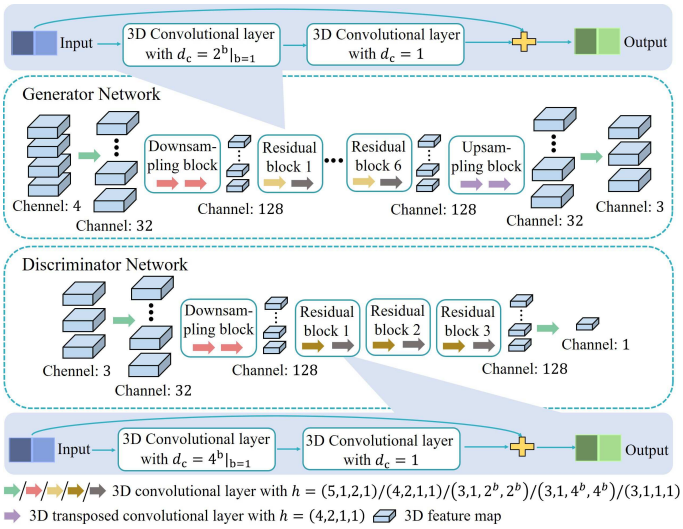

Fig. 2. The network structure of the proposed 3D-DCRGAN.

B. Off-Line Unsupervised Learning-Based Training Stage

We first define the cost function $V(D,G)$ of the 3D-DCRGAN, which is composed of a reconstruction loss $V_{\mathrm{L1}}(G)$ and an adversarial loss $V_{\mathrm{ad}}(D,G)$. Specifically, the reconstruction loss is equal to the L_1 loss integrated with weight $\widetilde{\boldsymbol{\Psi}}_{\mathrm{t}}$, i.e. $V_{\mathrm{L1}}(G) = \mathbb{E}_{\widetilde{\boldsymbol{\Psi}}}\left[\|\widetilde{\boldsymbol{\Psi}}_{\mathrm{t}} \odot (\widetilde{\boldsymbol{\Psi}}_{\mathrm{c}} - \widetilde{\boldsymbol{\Psi}}_{\mathrm{mc}})\|_1\right]$, where $\widetilde{\boldsymbol{\Psi}}_{\mathrm{mc}} = \mathbf{M}_{\mathrm{t}} \odot G(\mathbf{z}|\widetilde{\boldsymbol{\Psi}}_{\mathrm{c}}; \theta_g)$. The weight means that the importance of a measured gird scales with its measured RSS, since the signal coverage given by the radio map usually receives more attention than ambient noise. Moreover, we exploit the Wasserstein GAN with gradient penalty [17] to obtain the adversarial loss, i.e. $V_{\mathrm{ad}}(D,G) = \mathbb{E}_{\widetilde{\boldsymbol{\Psi}}}\left[D(\widetilde{\boldsymbol{\Psi}}_{\mathrm{c}}; \theta_d)\right] - \mathbb{E}_{\mathbf{z}}\left[D(\widetilde{\boldsymbol{\Psi}}_{\mathrm{mc}}; \theta_d)\right] - \lambda_{\mathrm{p}} GP(D)$, where the penalty coefficient $\lambda_{\mathrm{p}} = 10$ and the

[1]Although we can also obtain a two-channel gray-scale map by copying once to handle the confusion problem, a three-channel map is more useful for visualizing the reconstructed 3D radio map (i.e. a 3D heat map).

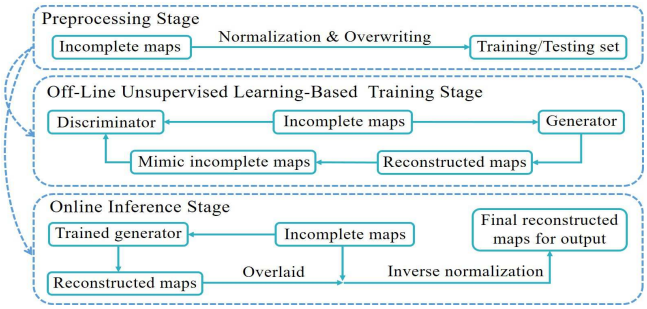

Fig. 3. The architecture of the proposed GAN-based 3D radio map reconstruction scheme.

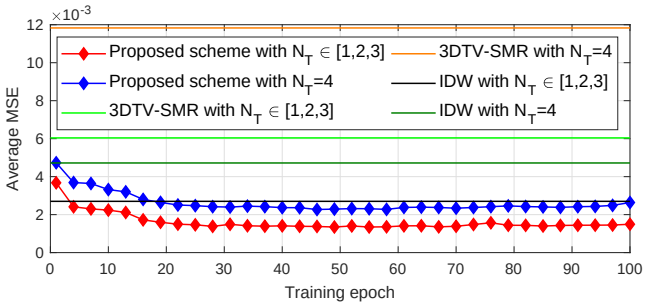

Fig. 4. Average MSE as a function of training epoch with different number N_{T} of transmitters, i.e. $N_{\mathrm{T}}=4$ or $N_{\mathrm{T}}\in[1,2,3]$

penalty item $GP(D)=\mathbb{E}_{\widetilde{\boldsymbol{\Psi}}'}\left[(\|\nabla_{\widetilde{\boldsymbol{\Psi}}'}D(\widetilde{\boldsymbol{\Psi}}';\theta_d)\|_2-1)^2\right]$. Note that the penalty map $\widetilde{\boldsymbol{\Psi}}'=\alpha\widetilde{\boldsymbol{\Psi}}_{\mathrm{c}}+(1-\alpha)\widetilde{\boldsymbol{\Psi}}_{\mathrm{mc}}$, where $\alpha\sim\mathcal{U}(0,1)$. The training of the 3D-DCRGAN essentially solves the problem of

$$\min_{\theta_g}\max_{\theta_d}V(D,G)=V_{\mathrm{ad}}(D,G)+\lambda_{\mathrm{r}}V_{\mathrm{L1}}(G), \tag{2}$$

where $\lambda_{\mathrm{r}}=1000$ is the reconstruction coefficient.

Given the above cost function in problem (2) and the incomplete maps obtained after the preprocessing stage, we borrow Algorithm 1 in [17] to train the 3D-DCRGAN. Specifically, in each iteration, N_{batch} incomplete maps are randomly selected from the training set and then input to the 3D-DCRGAN. Afterwards, the cost function related to the discriminator D or the generator G can be computed and exploited to perform error backpropagation and gradient-based learning [10]. Hence, the parameters θ_d and θ_g can be alternately updated, so as to maximize or minimize $V(D,G)$. After several training epochs on 3D-DCRGAN, we can obtain the trained 3D-DCRGAN that has captured the distribution of the RSS.

C. Online Inference Stage

In order to perform online 3D radio map reconstruction, we deploy the trained generator network of the 3D-DCRGAN for inference. Specifically, we first input the incomplete 3D radio map obtained in practice into the generator, yielding the reconstructed 3D radio map $G(\mathbf{z}|\widetilde{\boldsymbol{\Psi}}_{\mathrm{c}};\theta_g)=[\widehat{\boldsymbol{\Psi}}_{\mathrm{n}},\widehat{\boldsymbol{\Psi}}_{\mathrm{n}},\widehat{\boldsymbol{\Psi}}_{\mathrm{n}}]^T$, where $\widehat{\boldsymbol{\Psi}}_{\mathrm{n}}$ is a one-channel gray-scale reconstructed 3D radio map. Moreover, the value of each measured grid in the reconstructed map $\widehat{\boldsymbol{\Psi}}_{\mathrm{n}}$ is overlaid with the corresponding RSS in the incomplete map $\widetilde{\boldsymbol{\Psi}}_{\mathrm{n}}$, i.e. $\widehat{\boldsymbol{\Psi}}_{\mathrm{n}}=(\mathbf{1}-\mathbf{M}_{\mathrm{b}})\odot\widehat{\boldsymbol{\Psi}}_{\mathrm{n}}+\mathbf{M}_{\mathrm{b}}\odot\widetilde{\boldsymbol{\Psi}}_{\mathrm{n}}$. By performing inverse normalization, the final reconstructed 3D radio map for output can be obtained. The architecture of the proposed scheme is summarized in Fig. 3.

V. Performance Evaluation

In the simulations, the dimension $L\times W\times H$ of the target space $\mathbf{A}$ is set to $240\mathrm{m}\times240\mathrm{m}\times80\mathrm{m}$, and $\mathbf{A}$ is divided into $N_{\mathrm{L}}\times N_{\mathrm{W}}\times N_{\mathrm{H}}=48\times48\times16$ grids. Hence, the dimension $N_1\times N_2\times N_3$ of the small cube is equal to $4\times12\times12$. Moreover, we assume that there are 30000 and 10000 incomplete 3D radio maps in the training set and the testing set, respectively. For notational simplicity, we define a parameter set $q=(n,\sigma^2,\eta^2)$ of the radio map, where n, σ^2 and η^2 are the path loss exponent, the power of the addictive noise and the variance of the log-normal distribution, respectively. For the testing set, the parameter sets of all maps are set to $q=(6,-50,4)$. While for the training set, the parameter sets of every $10,000$ maps are set to $q=(8,-50,2)$, $q=(4,-50,0.5)$ and $q=(4,-30,2)$ in sequence. Furthermore, the reference distance is set to $d_0=10\mathrm{m}$. In addition, the learning rate and the batch size N_{batch} of 3D-DCRGAN are set to 0.0001 and 16, respectively.

For each 3D radio map, the transmitters are randomly placed on the ground (i.e. in the lowest 48×48 grids), and the transmit power (with unit of dBm) is randomly selected from the vector $[18.3,26.7,29.4,30,30,30,29.4,26.7,18.3]$. The number N_{T} of transmitters is randomly selected from 1 to 3, i.e. $N_{\mathrm{T}}\in[1,2,3]$. Moreover, the frequency point f of each map is randomly selected from $25\mathrm{MHz}$ to $125\mathrm{MHz}$. Under the configuration of constrained trajectories, we assume that the aircraft fly along 15 circle flight circuits at different altitudes (except for altitude at the lowest grids) with equal vertical intervals of $5\mathrm{m}$ and random radii unless otherwise stated. Given the same constrained trajectories, the IDW [6] and the 3DTV-SMR [9] algorithms are taken as baselines.

Fig. 4 investigates the average MSE as a function of training epoch with different number N_{T} of transmitters, where N_{T} with respect to the testing set satisfies $N_{\mathrm{T}}=4$ or $N_{\mathrm{T}}\in[1,2,3]$. It can be seen from Fig. 4 that regardless of the setting of N_{T}, the average MSE achieved by the proposed scheme decreases as training epoch increases and finally saturates at a value lower than that achieved by the baselines. Therefore, even if the number N_{T} of transmitters in the off-line training stage is different from that in the online inference stage, a 3D radio map can still be reconstructed with higher accuracy by the proposed scheme. The reason lies in that the captured distribution obtained by 3D-DCRGAN is nearly identical to the distribution of the RSS, thanks to the data-driven structure of DL and the unsupervised learning on 3D-DCRGAN.

Based on the proposed GAN-based scheme, Fig. 5 investigates the average MSE as a function of training epoch with different settings of cost function. As depicted in Fig. 5, the proposed 3D-DCRGAN without either the adversarial loss or the reconstruction loss suffers from a decrease in the average MSE of the reconstructed 3D radio map. This results from the fact that the adversarial loss and the reconstruction loss can enable GANs to capture more details about the distribution of the RSS in different ways. Specifically, from the generator's perspective, the adversarial loss aims to make the discriminator D difficult to discriminate between the actual incomplete

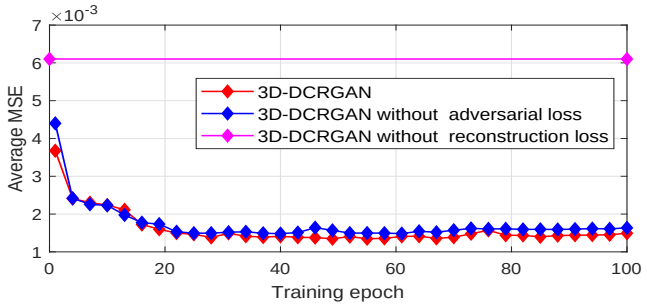

Fig. 5. Average MSE as a function of training epoch with different settings of cost function.

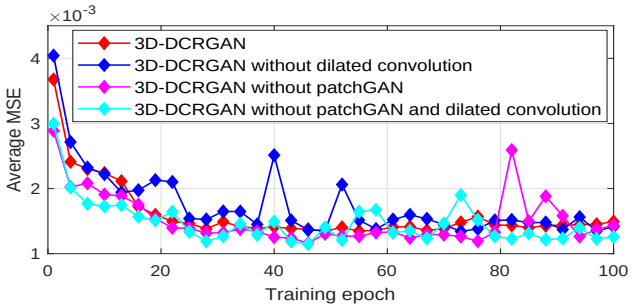

Fig. 6. Average MSE as a function of training epoch with different settings of network structure.

map $\widetilde{\mathbf{\Psi}}_{\mathrm{c}}$ and the mimic incomplete map $\widetilde{\mathbf{\Psi}}_{\mathrm{mc}}$, while the reconstruction loss tends to make each element in $\widetilde{\mathbf{\Psi}}_{\mathrm{c}}$ and the corresponding element in $\widetilde{\mathbf{\Psi}}_{\mathrm{mc}}$ yield similar value.

Similarly, Fig. 6 investigates the average MSE with different settings of network structure of the proposed 3D-DCRGAN. As shown in Fig. 6, the average MSE achieved by the proposed 3D-DCRGAN without dilated convolution and/or patchGAN dramatically fluctuates. Such a phenomenon means that it is difficult for these 3D-DCRGAN schemes to determine whether the average MSE is saturated, i.e. whether the reconstructed map can meet the accuracy requirement. On the contrary, with the aid of patchGAN and dilated convolution, the distribution of the RSS can be better captured by the proposed 3D-DCRGAN, improving the stability of the proposed scheme in terms of reconstruction accuracy.

In addition, we study the scenario where the aircraft may measure the RSS at fewer grids, i.e. the ratio of the measured space to the overall space is significantly small. To this end, the simulation of Fig. 7 assumes that aircraft fly only a quarter circle flight circuit at some selected altitudes, while fly a full circle at other altitudes. As depicted in Fig. 7, the average MSE achieved by the proposed scheme decreases with the growing number of full circle flight circuits but always lower than that achieved by the baselines. This illustrates that even if the amount of measured data for inference decreases, the proposed scheme can still provide more accurate reconstructed 3D radio maps than conventional algorithms.

VI. Conclusions

In this paper, we have studied a 3D radio map reconstruction problem, where incomplete maps are obtained by aircraft under constrained trajectories. A GAN-based 3D radio map reconstruction scheme consisting of preprocessing, off-line unsupervised learning-based training and online inference has been proposed, where 3D-DCRGAN is proposed to capture the distribution of the RSS. It is shown that benefiting from the sophisticatedly designed network structure and cost function, the proposed scheme can outperform various baselines in terms of the average MSE.

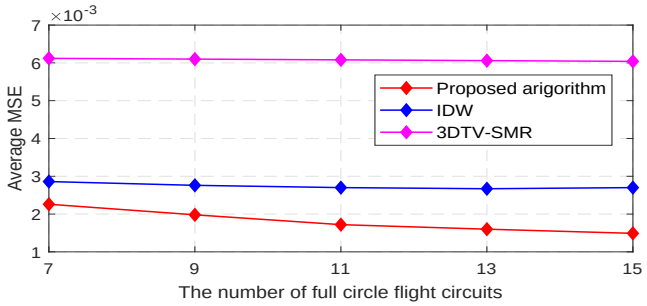

Fig. 7. Average MSE as a function of the number of full circle flight circuits.

References

[1] S. Bi, J. Lyu, Z. Ding, and R. Zhang, "Engineering radio maps for wireless resource management," *IEEE Wireless Commun.*, vol. 26, no. 2, pp. 133–141, 2019.

[2] J. Chen and D. Gesbert, "Efficient local map search algorithms for the placement of flying relays," *IEEE Transactions on Wireless Communications*, vol. 19, no. 2, pp. 1305–1319, 2019.

[3] W. Liu and J. Chen, "Geography-aware radio map reconstruction for uav-aided communications and localization," in *ICC 2021-IEEE International Conference on Communications*. IEEE, 2021, pp. 1–6.

[4] G. Ding, Q. Wu, L. Zhang, Y. Lin, T. A. Tsiftsis, and Y.-D. Yao, "An amateur drone surveillance system based on the cognitive Internet of Things," *IEEE Commun. Mag.*, vol. 56, no. 1, pp. 29–35, 2018.

[5] Q. Wu, J. Xu, Y. Zeng, D. W. K. Ng, N. Al-Dhahir, R. Schober, and A. L. Swindlehurst, "A Comprehensive Overview on 5G-and-Beyond Networks with UAVs: From Communications to Sensing and Intelligence," *J. Sel. Areas Commun.*, 2021.

[6] O. Huisman, R. De By *et al.*, "Principles of geographic information systems," *ITC Educational Textbook Series*, vol. 1, p. 17, 2009.

[7] K. Sato and T. Fujii, "Kriging-based interference power constraint: Integrated design of the radio environment map and transmission power," *IEEE Trans. Cogn. Commun. Netw.*, vol. 3, no. 1, pp. 13–25, 2017.

[8] A. Ivanov, V. Stoynov, K. Angelov, R. Stefanov, D. Atamyan, K. Tonchev, and V. Poulkov, "3D Interference Mapping for Indoor IoT Scenarios," in *Proc. Int. Conf. Telecommun. Signal Process. (TSP)*, 2020, pp. 265–269.

[9] Q. Wu, F. Shen, Z. Wang, and G. Ding, "3D Spectrum Mapping Based on ROI-Driven UAV Deployment," *IEEE Netw.*, vol. 34, no. 5, pp. 24–31, 2020.

[10] I. Goodfellow, J. Pouget-Abadie, M. Mirza, B. Xu, D. Warde-Farley, S. Ozair, A. Courville, and Y. Bengio, "Generative adversarial nets," in *Proc. Neural Inf. Process. Syst. (NIPS)*, 2014, pp. 2672–2680.

[11] K. Davaslioglu and Y. E. Sagduyu, "Generative adversarial learning for spectrum sensing," in *Proc. IEEE Int. Conf. Commun. (ICC)*, 2018, pp. 1–6.

[12] T. Hu, Y. Huang, Q. Zhu, and Q. Wu, "Channel Estimation Enhancement with Generative Adversarial Networks," *IEEE Trans. Cogn. Commun. Netw.*, vol. 7, no. 1, pp. 145–156, 2020.

[13] A. Pajot, E. de Bezenac, and P. Gallinari, "Unsupervised adversarial image reconstruction," in *Proc. Int. Conf. Learn. Represent. (ICLR)*, 2018.

[14] P. Isola, J.-Y. Zhu, T. Zhou, and A. A. Efros, "Image-to-image translation with conditional adversarial networks," in *Proc. IEEE/CVF Conf. Comput. Vis. Pattern Recognit. (CVPR)*, 2017, pp. 1125–1134.

[15] K. He, X. Zhang, S. Ren, and J. Sun, "Deep residual learning for image recognition," in *Proc. IEEE/CVF Conf. Comput. Vis. Pattern Recognit. (CVPR)*, 2016, pp. 770–778.

[16] F. Yu and V. Koltun, "Multi-scale context aggregation by dilated convolutions," *arXiv preprint arXiv:1511.07122*, 2015.

[17] I. Gulrajani, F. Ahmed, M. Arjovsky, V. Dumoulin, and A. C. Courville, "Improved training of wasserstein gans," in *Proc. Neural Inf. Process. Syst. (NIPS)*, 2017, pp. 5767–5777.